ACS APPLIED MATERIALS & INTERFACES

www.acsami.org

Research Article

Insights into the Construction of Robust Pt Clusters with Satisfactory Stability on CeO_2 for the Catalytic Oxidation of CO

Peng Yang, Chaoyi Luo, Wei Tan,* Qinglong Liu, Shaoxiong Zhang, Song Hong, Fei Gao,* and Lin Dong

Cite This: *ACS Appl. Mater. Interfaces* 2024, 16, 21782−21789

Read Online

ACCESS | Metrics & More | Article Recommendations | Supporting Information

ABSTRACT: Improving the efficiency of platinum group metals (Pt, Pd, Rh, etc.) in catalytic oxidation reactions remains an urgent topic. The conflict between the low-temperature activity and high-temperature stability of noble metals can hardly reach a consensus. For instance, Pt cluster catalysts supported on CeO_2 with high low-temperature activity will suffer from deactivation due to the redispersion under high-temperature lean-burn reaction conditions. Herein, two Pt_1/CeO_2 prepared by the incipient wetness impregnation method using different Pt precursors possessed varied Pt−O and Pt−O−Ce coordination numbers (CNs). They showed various priorities in CO oxidation versus NH_3 selective catalytic oxidation, materials with higher $CN_{Pt-O-Ce}$ selectively catalyzing NH_3 oxidation to N_2 more superior, conversely materials with lower $CN_{Pt-O-Ce}$ performing better in CO oxidation. After activation by H_2 reduction, both formed massive Pt clusters on the CeO_2 surface but showed drastically distinct stability in lean-burn CO oxidation reactions. By summarizing the experimental results of high-angle annular dark-field scanning transmission electron microscopy, X-ray absorption spectroscopy, Raman spectroscopy, *in situ* diffuse reflectance infrared Fourier transform spectroscopy, *etc.*, it is beyond doubt that the difference in the initial states of Pt_1 due to distinct precursors indeed determine the redispersion behavior of the reduced Pt clusters on CeO_2. Materials with lower $CN_{Pt-O-Ce}$ and higher CN_{Pt-O} are more likely to form robust Pt clusters, as they are not conducive to Pt anchoring, thus restricting the reversible structural evolution occurring under lean-burn CO oxidation and reductive conditions. This approach serves as a guide for the convenient and efficient construction and exploration of robust Pt cluster catalysts.

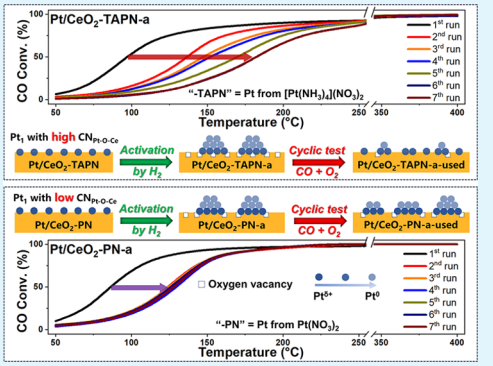

KEYWORDS: *robust Pt cluster catalysts, Pt−O−Ce coordination, Pt−CeO_2 interaction, precursor effects, lean-burn CO oxidation*

1. INTRODUCTION

Pt single atom supported on CeO_2 (Pt_1/CeO_2) with a 100% atomic utilization efficiency could be easily prepared by the (incipient) wetness impregnation method in industry and exhibited superior stability. However, Pt_1 generally underperformed Pt clusters/particles in the catalytic oxidation of air pollutants (*e.g.*, CO and hydrocarbons) due to the overstability of Pt_1 limiting the activation of oxygen at low temperatures.[1,2] Consequently, constructing highly active and stable Pt cluster catalysts on CeO_2-based supports is still a research hotspot for the environmental catalysis community.

Over the decades, performing reduction treatment on Pt/CeO_2 catalysts at appropriate temperatures to form homogeneous Pt clusters/particles has been one of the most facile and industrially practical methods to enhance their catalytic oxidation performance.[1,3] With the development of characterization techniques, the surface reduction process could be described as the reduction of PtO_x species (or even Pt_1-O_x sites) and adjacent Ce^{4+} sites, accompanied by the possible aggregation of Pt species and the formation of Ce^{3+}/oxygen vacancies. Nevertheless, those highly active Pt clusters/particles generated by reduction treatment might be reoxidized and redispersed into less active Pt_1 or smaller PtO_x clusters in O_2 or even under lean reaction conditions at elevated temperatures.[3−5] This severely limited the application of Pt cluster catalysts in harsh environments. Therefore, it is desirable and urgent to develop a facile but effective strategy for fabricating highly active and stable Pt clusters supported on CeO_2 for the catalytic oxidation of air pollutants under lean conditions in large-scale industrial production.

Previously, we reported the substantial influence of the valence and the local coordination environment of Pt_1 supported on CeO_2 on its catalytic performance before and after activation treatment, and distinct Pt−CeO_2 interactions would also influence the process of reduction and aggregation

Received: January 7, 2024
Revised: March 13, 2024
Accepted: April 9, 2024
Published: April 18, 2024

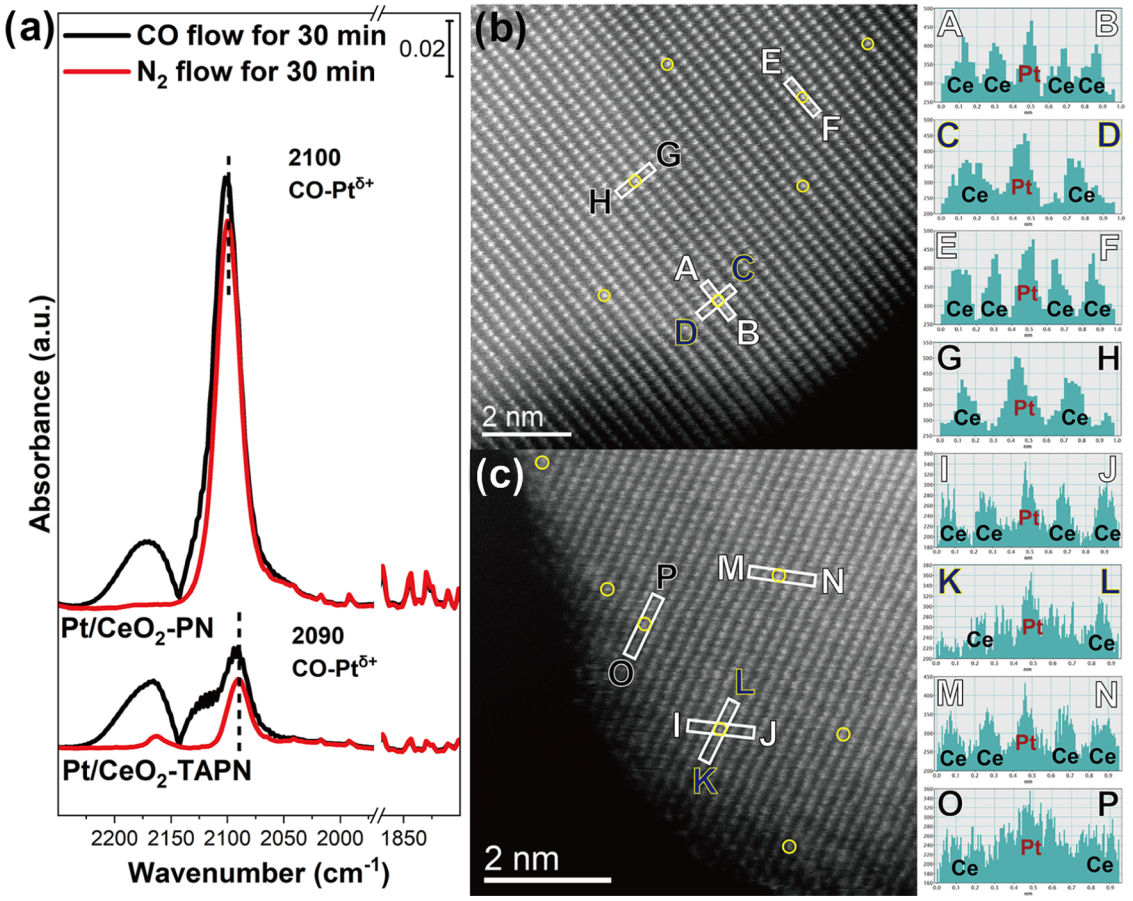

Figure 1. Atomically dispersed Pt on CeO_2. (a) *In situ* DRIFTS of CO adsorption on Pt/CeO_2−TPAN and Pt/CeO_2−PN at 30 °C. HAADF-STEM images and line profiles of (b) Pt/CeO_2−TAPN and (c) Pt/CeO_2−PN.

of Pt species, resulting in differences in the size of the reduced Pt clusters. It indicated that the initial states of Pt_1 would also determine the surface structure evolution process during the reduction treatment and the final structure of the generated Pt clusters.[2,6] Based on this understanding, it was inferred that Pt clusters evolving from Pt_1 with varying initial states, induced by reduction treatment, might also manifest divergent stability characteristics under lean conditions.

Herein, we disclosed that two widely used Pt precursors (i.e., tetraamineplatinum(II) nitrate and platinum(II) nitrate) had a critical impact on the characteristics of CeO_2-supported Pt_1, including the valence and local coordination environment, *etc.* Moreover, the two different Pt_1/CeO_2 catalysts showed a significant bias toward various catalytic oxidation reactions (CO oxidation vs NH_3 oxidation) due to their different Pt_1 coordination environments with different Pt−O−Ce quantities, illustrating the significance of the synthesis process and the gap of nature between both. More interestingly, after identical reduction treatment, despite the similar size and low-temperature oxidative activity of the Pt clusters on the two catalysts, Pt clusters derived from Pt_1 using distinct Pt precursors exhibited quite contrasting stability in lean CO oxidation reactions.

2. MATERIALS AND EXPERIMENTAL METHODS

2.1. Catalyst Preparation. To prepare CeO_2, a certain amount of $Ce(NH_4)_2(NO_3)_6$ was dissolved in deionized water. Excess $NH_3{\cdot}H_2O$ aqueous solution was added to the solution with vigorous stirring until the pH reached 10. The resulting mixture was then aged overnight, filtered, and washed several times with deionized water at ambient temperature. The obtained precipitate was dried at 100 °C for 12 h and subsequently calcined at 550 °C for 2 h in air with a ramping rate of 5 °C min^{-1}.

1 wt. % Pt was loaded onto CeO_2 by the incipient wetness impregnation (IWI) method, where tetraamineplatinum(II) nitrate ($Pt(NH_3)_4(NO_3)_2$, TAPN) and platinum(II) nitrate ($Pt(NO_3)_2$, PN) solution obtained from Aladdin were used as Pt precursors. After impregnation with a TAPN or PN solution, the obtained Pt/CeO_2 powders were dried at 120 °C for 30 min and then calcined at 550 °C for 2 h in air. The obtained samples were denoted as Pt/CeO_2−TAPN and Pt/CeO_2−PN. Before each test of the activated catalyst, the original material was reduced with 7% H_2/Ar at 400 °C for 1 h and denoted with "-a" (-a = after activation by H_2 reduction). The activated samples collected after the activity of the CO oxidation cycle reaction stabilized will be designated as "-u" (-u = used under the high-temperature lean condition).

2.2. Catalytic Activity Measurements. CO oxidation: approximately 15 mg of sample (40−60 mesh) was used in each CO oxidation test, attenuated by 150 mg of SiC to minimize the thermal effect. The total flow rate was 50 mL min^{-1} with a weight hourly space velocity (WHSV) of 200,000 mL g_{cat}^{-1} h^{-1} with a feed gas of 1% CO and 1% O_2 in He balanced. The catalytic oxidation was reacted in a fixed-bed reactor. CO and CO_2 in the reaction exhaust were converted to CH_4 by a commercial Ni catalyst at 350 °C and quantified by a flame ionization detector (FID) equipped with online gas chromatography.

The CO conversion is calculated by

$$\text{CO conversion} = \left(1 - \frac{[\text{CO}]_{\text{out}}}{[\text{CO}]_{\text{in}}}\right) \times 100\%$$

https://doi.org/10.1021/acsami.4c00342
ACS Appl. Mater. Interfaces 2024, 16, 21782−21789

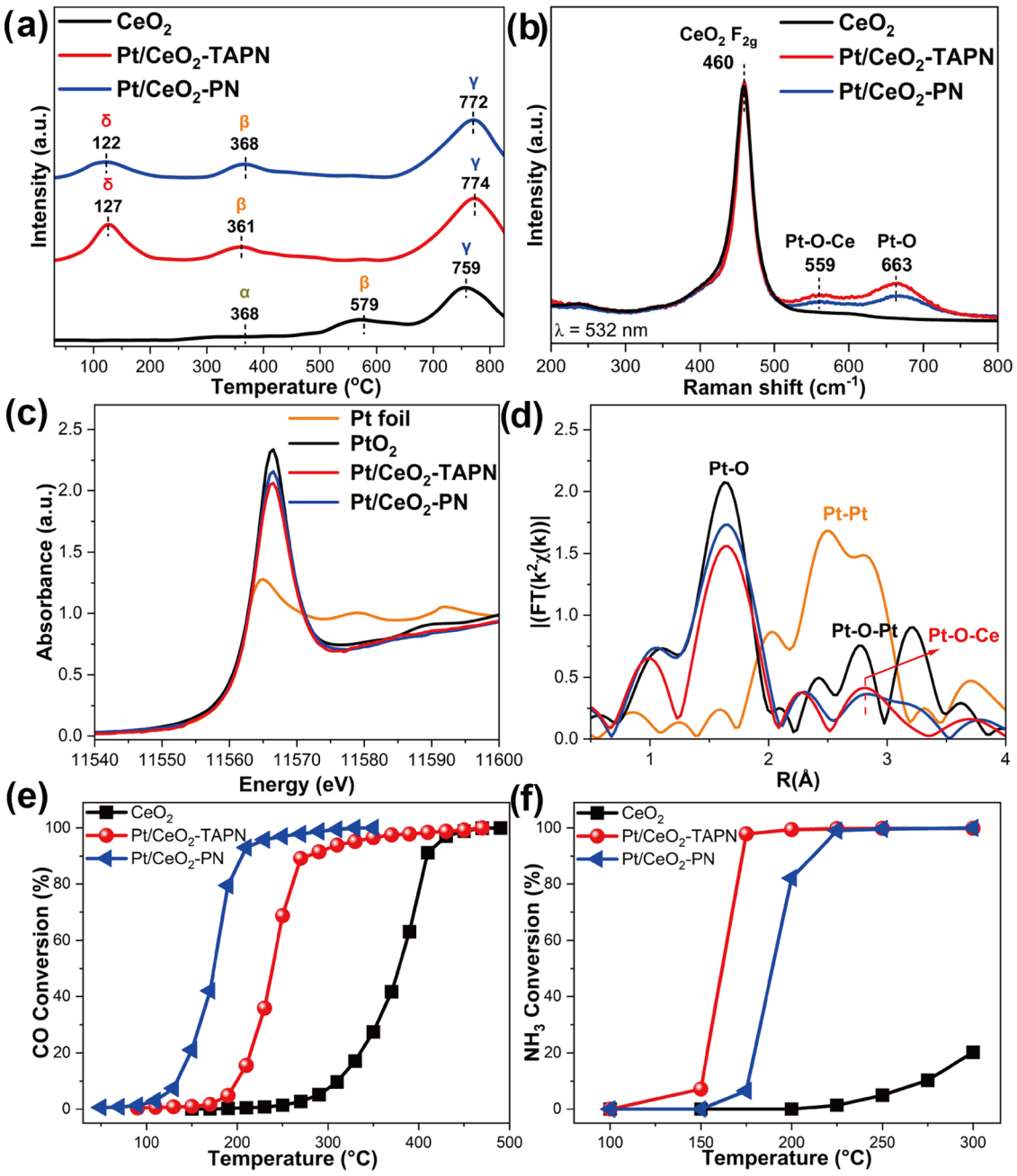

Figure 2. Different Pt_1 sites on CeO_2 and their catalytic oxidation performance. (a) H_2-TPR profiles and (b) Raman spectroscopy for CeO_2, Pt/CeO_2−TAPN, and Pt/CeO_2−PN; (c) normalized XANES and (d) EXAFS magnitude of the Fourier-transformed k^2-weighted $\chi(k)$ data for Pt/CeO_2−TAPN and Pt/CeO_2−PN at the Pt-L_3 edge with Pt foil and PtO_2 as references; (e) CO oxidation activity and (f) NH_3 oxidation activity on CeO_2, Pt/CeO_2−TAPN, and Pt/CeO_2−PN (reaction condition: $[O_2]$ = 1%, [CO] = 1% or $[NH_3]$ = 500 ppm, balanced with He, WHSV = 200,000 mL g_{cat}^{-1} h^{-1}).

For the NH_3 oxidation activity test, the reactants consisted of 500 ppm of NH_3 and 1% O_2 in Ar balanced. The WHSV was controlled at 200,000 mL g_{cat}^{-1} h^{-1}. The concentrations of NH_3, NO, NO_2, and N_2O in the effluent gas were measured by an online Thermo Nicolet iS10 Fourier transform infrared (FTIR) spectrometer. All reactions were performed under steady-state conditions. The NH_3 conversion and N_2 selectivity in the NH_3 oxidation reaction were calculated according to the following equations

$$\text{NH}_3\ \text{conversion} = \left(1 - \frac{[\text{NH}_3]_{\text{out}}}{[\text{NH}_3]_{\text{in}}}\right) \times 100\%$$

$$\text{NH}_3\ \text{selectivity} = \left(1 - \frac{[\text{NO}]_{\text{out}} + [\text{NO}_2]_{\text{out}} + 2[\text{N}_2\text{O}]_{\text{out}}}{[\text{NH}_3]_{\text{in}} - [\text{NH}_3]_{\text{out}}}\right) \times 100\%$$

In the CO oxidation cyclic reaction test of the activated samples, the sample was heated to 400 °C by temperature programming and then maintained for 1 h with a continuous feed gas consisting of 1% CO and 1% O_2 in He balanced. Afterward, the fixed-bed reactor naturally cooled to ambient temperature and being exposed to air for 10 min, where the above process was set up as a complete cyclic reaction activity test. The test was run until the last two activity curves were stable.

https://doi.org/10.1021/acsami.4c00342
ACS Appl. Mater. Interfaces 2024, 16, 21782−21789

In the study of the CO oxidation reaction kinetics, to avoid the heat and mass transfer effects, the reaction rates were determined with CO conversions below 10%, and the samples (40−60 mesh) were mixed with SiC (with a mass ratio of 1:20) before the test to minimize the effect. For the reaction order test, the feed gas consisted of 1% CO and 1% O_2 in He balanced. The WHSV was controlled at 300,000 and 60,000 mL g_{cat}^{-1} h^{-1} for Pt/CeO_2−PN and Pt/CeO_2−TAPN, respectively.

2.3. Characterizations. Details of the characterizations are described in Supporting Information (SI) Text S1.

3. RESULTS AND DISCUSSION

3.1. Identification and Properties of Pt_1/CeO_2. As stated in Text S1 (Supporting Information), Pt/CeO_2 catalysts using tetraamineplatinum(II) nitrate and platinum(II) nitrate as Pt precursors were prepared by the conventional incipient wetness impregnation (IWI) method, denoted as Pt/CeO_2−TAPN and Pt/CeO_2−PN, respectively. Considering that the kinds of precursors had a significant impact on ion adsorption, dispersion, and the final local structure of the deposited species during the synthesis,[7,8] the possible difference in the surface structure of Pt/CeO_2−TAPN and Pt/CeO_2−PN was first investigated systematically. As shown in Figure S1 and Table S1 (Supporting Information), after the loading of Pt, there were no significant alterations in the specific surface area and the pore structure of CeO_2, and no crystalline Pt or PtO_x was detected, implying that Pt species were highly dispersed on the CeO_2 support, regardless of the Pt precursors. To further determine the dispersion states of Pt species, *in situ* diffuse reflectance infrared Fourier transform spectroscopy (DRIFTS) of CO adsorption was conducted (Figure 1a). For both Pt/CeO_2−TAPN and Pt/CeO_2−PN, only a highly symmetric band assigned to CO adsorbed on ionic isolated Pt sites (CO−$Pt^{\delta+}$) was observed at *ca.* 2095 cm^{-1} after N_2 purge without bridge CO at 1800−1850 cm^{-1},[1,9] indicating that Pt species on Pt/CeO_2−TAPN and Pt/CeO_2−PN primarily existed as single atoms. Remarkably, the center of the CO−$Pt^{\delta+}$ bands on Pt/CeO_2−TPAN and Pt/CeO_2−PN differed by 10 cm^{-1} in position (2090 vs 2100 cm^{-1}), and the intensity of the CO band on Pt/CeO_2−PN significantly surpassed that on Pt/CeO_2−TAPN, hinting variations in valence states or coordination environments of Pt on these two Pt/CeO_2 catalysts. As demonstrated by the high-angle annular dark-field scanning transmission electron microscopy (HAADF-STEM) images of Pt/CeO_2−TPAN and Pt/CeO_2−PN (Figure 1b,c), no obvious Pt agglomerates were observed, and some isolated Pt atoms could be identified with the aid of line profile analysis, further confirming that Pt species on both Pt/CeO_2−TAPN and Pt/CeO_2−PN were predominantly in the form of single atoms. Energy-dispersive spectroscopy (EDS)-mapping results also corroborated that Pt species were highly dispersed on the prepared Pt catalysts (Figure S2, Supporting Information). Furthermore, considering that the practical Pt loadings on Pt/CeO_2−TAPN (0.90 wt. %) and Pt/CeO_2−PN (0.93 wt. %) determined by inductively coupled plasma-optical emission spectrometry (ICP-OES) were almost the same and Pt species were all atomically dispersed, the significant differences in the intensity and the position of CO bands in DRIFTS study should be attributed to the local coordination environment and valence of Pt.

Aimed at disclosing the difference in the surface microstructure and the states of Pt species on Pt/CeO_2−TAPN and Pt/CeO_2−PN, additional characterizations were conducted. Besides assessing the redox properties of catalysts, H_2-TPR could also serve to investigate the surface structure of Pt/CeO_2 catalysts. As shown in Figure 2a, the H_2-consumption peaks at 50−200 °C could be attributed to the reduction of surface Pt−O and Pt−O−Ce species, while the H_2-consumption peaks around 365 and 770 °C were assigned to that of surface Ce^{4+} species and bulk CeO_2, respectively.[10] The relatively higher intensity of the H_2-consumption peak related to the Pt−O(−Ce) structure on Pt/CeO_2−TAPN suggested the formation of more Pt−O−Ce linkages, which was further confirmed by peak fitting analysis (Figure S3 and Table S2, Supporting Information). The slightly higher reduction temperature of the Pt−O(−Ce) structure on Pt/CeO_2−TAPN than that on Pt/CeO_2−PN might be due to the enhanced Pt−CeO_2 interaction on Pt/CeO_2−TAPN. Raman spectroscopy, a powerful tool to probe the surface structure of Pt/CeO_2 catalysts, was also conducted on the CeO_2 support and Pt/CeO_2. As shown by the normalized Raman spectroscopy for CeO_2, Pt/CeO_2−TAPN, and Pt/CeO_2−PN (Figure 2b), the bands ascribed to Pt−O−Ce and Pt−O (in Pt−O−Ce) structures on Pt/CeO_2−TAPN were more intensive than those on Pt/CeO_2−PN, further confirming the formation of more Pt−O−Ce structures on Pt/CeO_2−TAPN.[4,11]

X-ray absorption spectroscopy (XAS) analysis was used to further elucidate the valence and local coordination environment of Pt_1 on the prepared Pt/CeO_2 catalysts. The white line intensity of Pt-L_3 X-ray absorption near-edge structure (XANES) followed an order of PtO_2 > Pt/CeO_2−PN > Pt/CeO_2−TAPN > Pt foil (Figure 2c), suggesting that the valence of Pt on Pt/CeO_2 catalysts was between 0 and +4, and Pt species on Pt/CeO_2−PN showed a slightly higher valence than Pt/CeO_2−TAPN, supported by the results of XPS (Table S4, Supporting Information). To further reveal the local coordination environment of Pt species on Pt_1/CeO_2 catalysts, the extended X-ray absorption fine structure (EXAFS) data were processed and plotted (Figure 2d and Table S3, Supporting Information). The absence of Pt−Pt and Pt−O−Pt shells on both Pt/CeO_2−TAPN and Pt/CeO_2−PN proved that the Pt species on these two catalysts were in the form of single atoms. Moreover, even though the coordination number (CN) of Pt−O on Pt/CeO_2−TAPN was lower than that of Pt/CeO_2−PN, it showed a higher $CN_{Pt-O-Ce}$, which was consistent with H_2-TPR, Raman spectroscopy, and XPS that more Pt−O−Ce linkages were formed on Pt/CeO_2−TAPN and Pt species on it showed lower valence. Such counterintuitive results might be related to more Pt_1 embedded into the surface lattice or anchored on the step sites on Pt/CeO_2−TAPN in a Pt−O_4 configuration.[12,13] Together with the more significant CeO_2 lattice shrinkage on Pt/CeO_2−TAPN than Pt/CeO_2−PN as suggested by X-ray diffraction (XRD) pattern Rietveld refinement (Figure S5, Supporting Information), it could be proposed that a certain amount of Pt with smaller ionic radius (Pt^{4+} = 0.625 Å, Pt^{2+} = 0.800 Å) than Ce^{3+}/Ce^{4+} (Ce^{4+} = 0.970 Å, Ce^{3+} = 1.280 Å) on Pt/CeO_2−TAPN were embedded into the surface lattice of CeO_2, resulting in the higher $CN_{Pt-O-Ce}$ and stronger Pt−CeO_2 interaction.[9,14]

3.2. Catalytic Performance in NH_3 and CO Oxidation. CO oxidation was one of the best-known probe reactions in the heterogeneous catalysis field.[15] Herein, the CO oxidation activity on Pt/CeO_2−TAPN and Pt/CeO_2−PN was also measured to help understand their structure and evaluate their potential in the catalytic oxidation of air pollutants. As shown in Figure 2e, the deposition of Pt significantly bolstered the CO oxidation activity on CeO_2. Furthermore, Pt/CeO_2−PN

https://doi.org/10.1021/acsami.4c00342
ACS Appl. Mater. Interfaces 2024, 16, 21782−21789

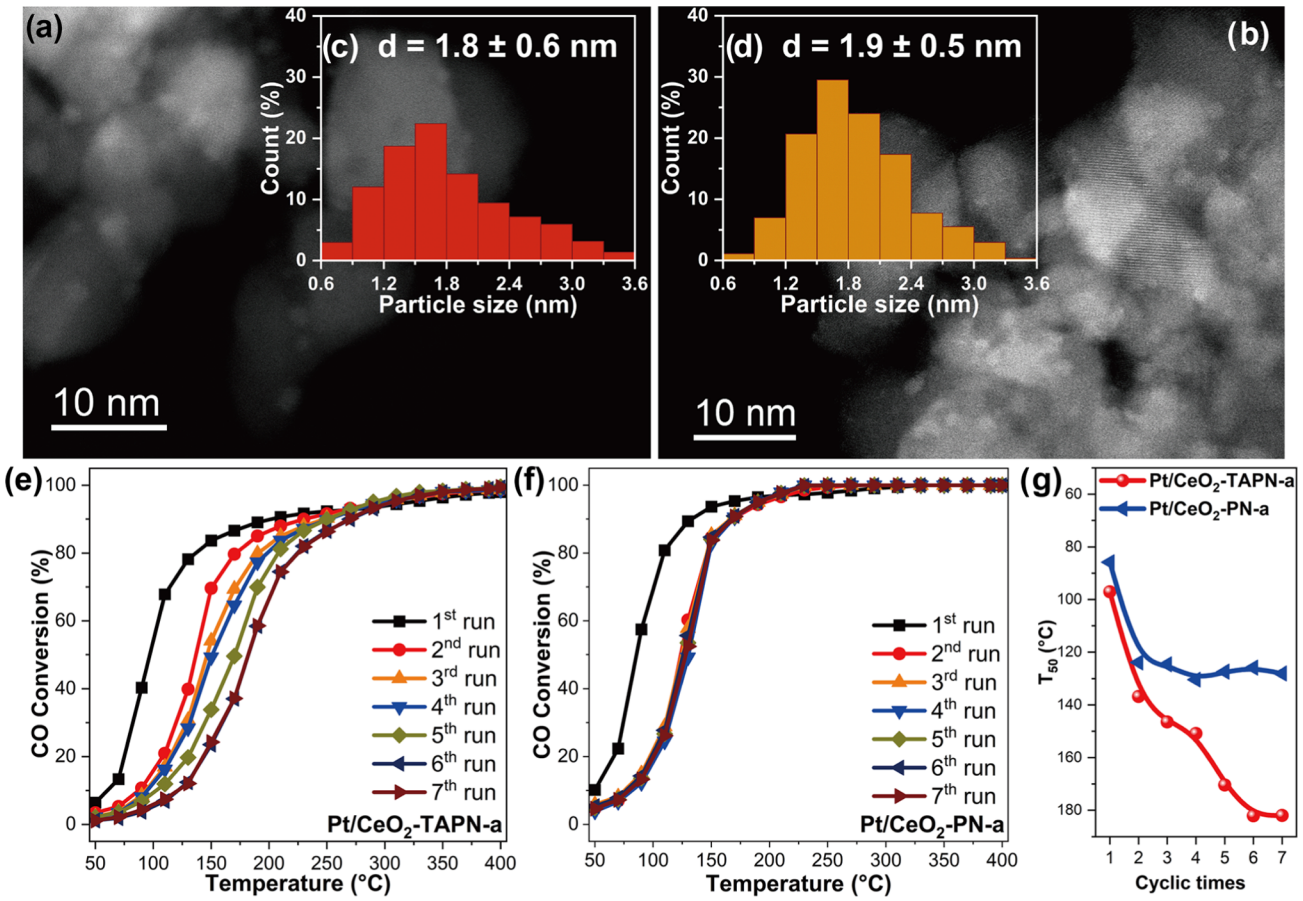

Figure 3. Pt cluster catalysts generated by H_2 reduction and their reactivity and stability in CO oxidation under lean-burn condition. HAADF-STEM images of (a, c) Pt/CeO_2−TAPN-a and (b, d) Pt/CeO_2−PN-a and the size distribution of Pt clusters/particles within them; CO oxidation activity on (e) Pt/CeO_2−TAPN-a and (f) Pt/CeO_2−PN-a in cyclic CO oxidation test under lean-burn condition (7-round test, from RT to 400 °C; reaction condition: [CO] = [O_2] = 1%, balanced with He, WHSV = 200,000 mL g_{cat}^{-1} h^{-1}); and (g) the variation of T_{50} on Pt/CeO_2−TAPN-a and Pt/CeO_2−PN-a in the cyclic CO oxidation test.

showed higher activity and lower activation energy (E_a) than Pt/CeO_2−TAPN in the CO oxidation reaction (Figures 2e and S6, Supporting Information), indicating the different states of Pt_1 on them. The strikingly distinct reaction orders for CO and O_2 on Pt/CeO_2−TAPN (0.75/0.11) and Pt/CeO_2−PN (0.11/0.27) further proved the diverse local coordination environments of Pt_1 on these two catalysts (Figure S7, Supporting Information), resulting in the distinctive features in CO adsorption and O_2 activation (Figure S8, Supporting Information). Recently, we have also reported that Pt_1/CeO_2 with higher $CN_{Pt-O-Ce}$ due to the formation of surface lattice-embedded Pt_1 sites would exhibit lower CO oxidation activity but enhanced NH_3 oxidation activity compared with those with lower $CN_{Pt-O-Ce}$.[9] Inspired by this, the NH_3 oxidation reaction was also used as a probe reaction to understand the local coordination environments of Pt_1 on Pt/CeO_2−TAPN and Pt/CeO_2−PN. As expected, Pt/CeO_2−TAPN with higher $CN_{Pt-O-Ce}$ showed much higher NH_3 oxidation activity than Pt/CeO_2−PN with relatively lower $CN_{Pt-O-Ce}$ (Figure 2f). Based on the characterizations and catalytic performance evaluation, it could be concluded that the local coordination environment of Pt_1 on CeO_2 prepared by the conventional IWI method could be fine-tuned by choosing different Pt precursors to obtain Pt_1/CeO_2 with different $CN_{Pt-O-Ce}$ for diverse catalytic oxidation reactions or the following processes.

Considering that the CO oxidation activity on both Pt/CeO_2−TAPN and Pt/CeO_2−PN was far away from the "150 °C challenge" (CO conversion reached 90% by 150 °C) set for vehicle emission control,[16] a reduction treatment by H_2 at 400 °C was conducted on the prepared Pt_1/CeO_2 catalysts to improve their CO oxidation activity. As shown in Figure 3a,3b, after activation by H_2 reduction, abundant Pt clusters were formed on Pt/CeO_2−TAPN-a and Pt/CeO_2−PN-a. The comparable average size of Pt clusters on Pt/CeO_2−TAPN-a (1.8 ± 0.6 nm) and Pt/CeO_2−PN-a (1.9 ± 0.5 nm) should be due to the similar reduction temperature of the Pt−O−Ce structure in the H_2 atmosphere as well as the same CeO_2 support. In line with expectations, H_2 activation significantly promoted the low-temperature catalytic oxidation performance of Pt_1/CeO_2. To further investigate the stability of Pt cluster catalysts under realistic reaction conditions (lean-burn), cyclic tests were conducted. It was not surprising that Pt/CeO_2−TAPN-a experienced severe deactivation over 7 cycles, with T_{50} (the temperature at which CO conversion reached 50%) increasing from 97 to 182 °C (Figure 3g). In clear contrast, a much lesser increase in T_{50} was observed on Pt/CeO_2−PN-a after the first round of testing, with T_{50} increasing from 86 to 124 °C. In the following cyclic test, Pt/CeO_2−PN-a demonstrated superior stability without further deactivation.

3.3. Robust Pt Cluster Catalysts. Previous reports have indicated that excessive gaseous oxygen under lean-burn

https://doi.org/10.1021/acsami.4c00342
ACS Appl. Mater. Interfaces 2024, 16, 21782−21789

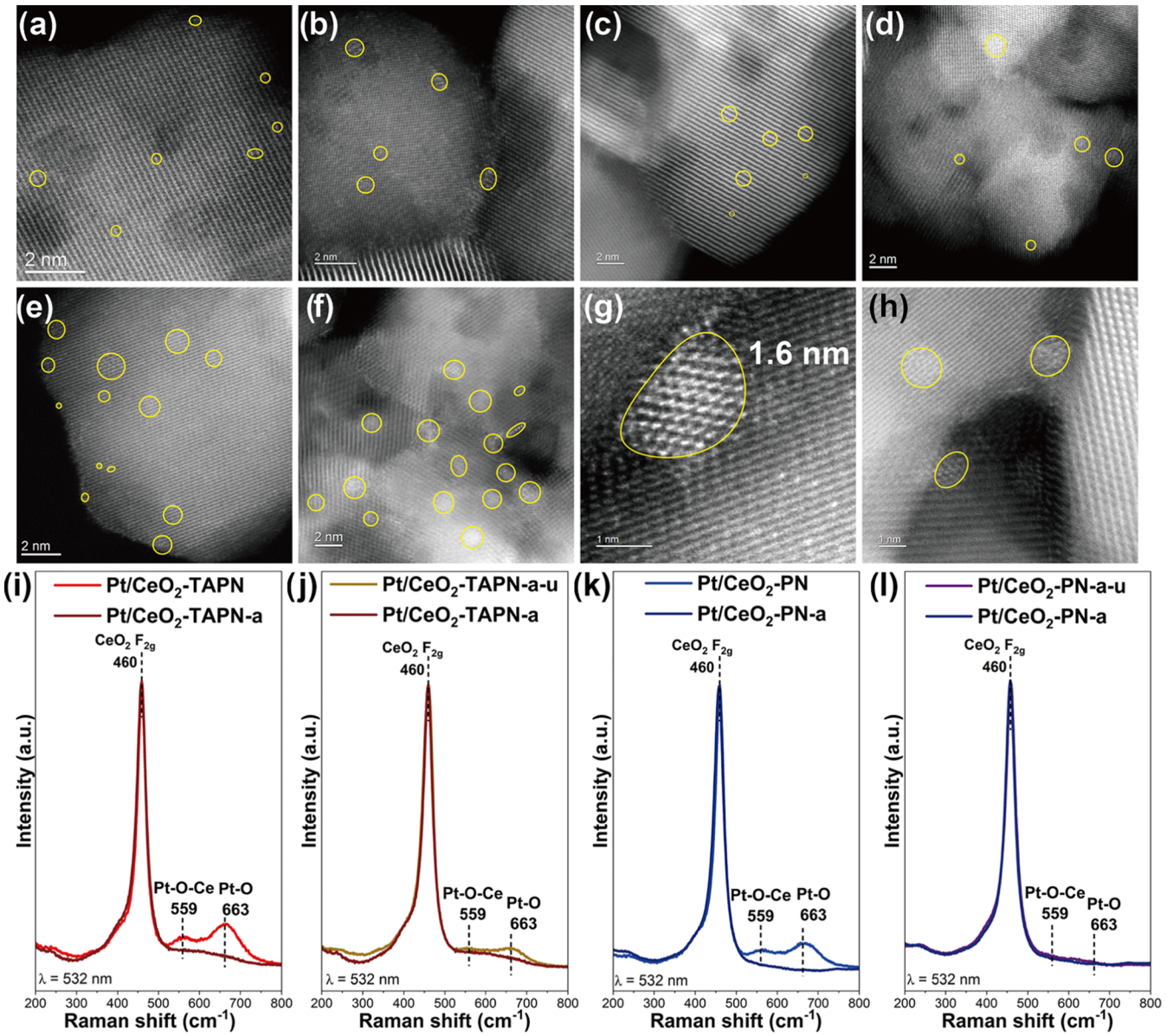

Figure 4. State of Pt species on the used Pt/CeO_2-a surface. HAADF-STEM images of (a–d) used Pt/CeO_2–TAPN-a and (e–h) Pt/CeO_2–PN-a (some Pt sites were identified by yellow circles); (i–l) Raman spectroscopy for as-prepared, activated, and used Pt/CeO_2 catalysts.

conditions would result in the redispersion of Pt clusters on CeO_2-based supports at elevated temperatures, especially those constructed by reduction treatments, thereby limiting their industrial applicability.[4,5] To further elucidate the reasons for the different stabilities of Pt cluster catalysts derived from Pt_1/CeO_2 using various Pt precursors, *in situ* DRIFTS of CO adsorption was conducted on fresh and used Pt catalysts ("used" meant Pt catalysts used in cyclic tests without further deactivation). As shown in Figures S9 and S10 (Supporting Information), IR bands assigned to CO linearly adsorbed on $Pt^{\delta+}$ ($CO–Pt^{\delta+}$, $Pt^{\delta+}$ = Pt_1 or Pt in small PtO_x clusters) and metallic Pt clusters/particles ($CO–Pt^0$) were observed on both activated catalysts before and after the cyclic CO oxidation test.[1,2] It was found that the intensity of the $CO–Pt^{\delta+}$ and $CO–Pt^0$ bands on Pt/CeO_2–TAPN-a increased and decreased after the cyclic test, respectively, suggesting that significant redispersion and reoxidation of Pt clusters/particles might have occurred on Pt/CeO_2–TAPN-a. By contrast, a limited change was observed in the intensity of the $CO–Pt^{\delta+}$ and the $CO–Pt^0$ bands on Pt/CeO_2–PN-a. Given that Pt/CeO_2–TAPN-a was much more severely deactivated than Pt/CeO_2–PN-a, and Pt^0 sites on Pt clusters/particles were the main reactive sites in the CO oxidation reaction, Pt clusters/particles on Pt/CeO_2–PN-a were more stable than those on Pt/CeO_2–TAPN-a under lean-burn conditions.

To further investigate the redispersion of aggregated Pt species after the cyclic test, HAADF-STEM images for used Pt/CeO_2–TAPN-a and Pt/CeO_2–PN-a were captured (Figures 4a–4h, and S11, Supporting Information). Although identifiable Pt clusters still could be found on used Pt/CeO_2–TAPN-a and Pt/CeO_2–PN-a, the particle sizes of Pt clusters on them seemed to have decreased. Moreover, more Pt clusters with large size (>1.0 nm) could be observed on used Pt/CeO_2–PN-a compared with those of used Pt/CeO_2–TAPN-a (*ca.* 0.5 nm), and some Pt single atoms were even found on used Pt/CeO_2–TAPN-a, further confirming that the redispersion of Pt clusters occurred during the cyclic test and Pt clusters on Pt/CeO_2–PN-a showed better stability. Raman

https://doi.org/10.1021/acsami.4c00342
ACS Appl. Mater. Interfaces 2024, 16, 21782–21789

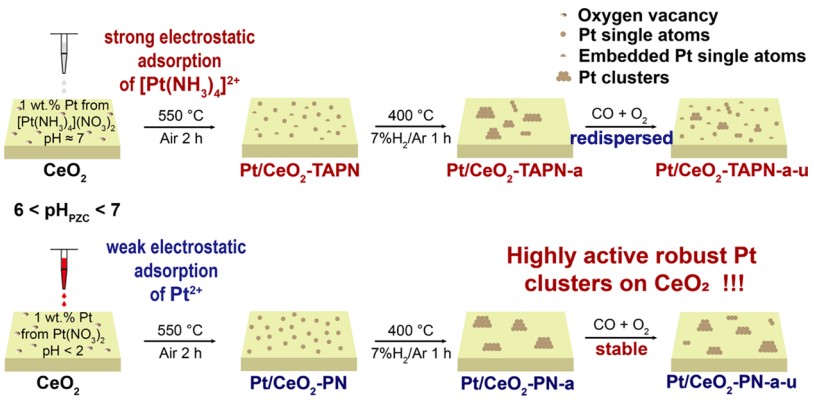

Figure 5. Formation of robust Pt clusters on CeO_2. Schematic illustration of catalyst preparation and the surface structure evolution of Pt/CeO_2 during the calcination, activation, and catalytic performance evaluation process.

spectroscopy was used to investigate the structure evolution from the perspective of the Pt−O−Ce structure (Figure 4i−l). The bands assigned to the Pt−O−Ce structure on Pt/CeO_2 almost vanished after the reduction treatment, indicating that ionic Pt single atoms on these two catalysts aggregated into metallic Pt clusters/particles. After the cyclic test, exclusive Raman bands assigned to the Pt−O−Ce/Pt−O structure emerged on the used Pt/CeO_2−TAPN-a, suggesting the redispersion of Pt clusters. Differently, weaker bands related to the Pt−O−Ce structure were found on used Pt/CeO_2−PN-a, strongly supporting that Pt clusters on Pt/CeO_2−PN-a were highly stable under that reaction condition.

3.4. Mechanism of Pt Cluster Stability. Based on the summary of the aforementioned data, we found that merely changing the precursor as a variable resulted in a change in the nature of Pt_1 in the Pt/CeO_2 catalysts. The mutual corroboration between the various characterization results and catalytic activities illustrated the difference in the Pt_1 coordination environments between Pt/CeO_2−TAPN and Pt/CeO_2−PN, which ultimately determines from the results the stability of the Pt cluster catalysts formed by the two catalysts after reduction.

Combining the results of characterizations and catalytic performance evaluation, we could propose the surface structure evolution process in Figure 5. According to the previous report on the strong electrostatic adsorption (SEA) method, it could be inferred that different pH values of the Pt precursor solution could markedly affect the electrostatic adsorption process during the synthesis, thus generating varied final states of adsorbed species on the supports. In particular, the aqueous solution of TAPN was neutral, and its pH value was above the point of zero charge (PZC) of CeO_2, which made the hydroxyl groups on CeO_2 deprotonated and negatively charged, thus benefiting the adsorption of $[Pt(NH_3)_4]^{2+}$. However, for Pt/CeO_2−PN, the acidic solution of PN (pH < 2) would result in the protonation of hydroxyl groups on CeO_2, which would partially inhibit the adsorption of Pt^{2+} cations.[1,17] That is why more Pt−O−Ce linkages and stronger Pt−CeO_2 interaction were formed on Pt/CeO_2−TAPN than on Pt/CeO_2−PN. As suggested by the results of H_2-TPR, the higher concentration of the Pt−O−Ce structure on Pt/CeO_2−TAPN could induce more drastic surface reduction during the H_2 treatment and the generation of more surface defects. Such high-density surface defects could facilitate the redispersion of Pt clusters/particles and the anchoring of Pt atoms, well supported by the most recent report that the initial coordination environment of Pt_1 could create memory on the CeO_2 support where the Pt atoms returned under lean CO oxidation or oxidative conditions, potentially providing a catalyst self-healing after the reduction treatment.[5] Relatively mild surface reduction processes on Pt/CeO_2−PN and the formation of fewer surface defects should be the main reason for the better stability of Pt clusters/particles on Pt/CeO_2−PN-a under lean-burn conditions.

4. CONCLUSIONS

In conclusion, *via* the adoption of different Pt precursors, the initial local coordination environments of Pt_1 on CeO_2 could be finely tuned by a conventional IWI method. Electrostatic adsorption of diverse precursors during synthesis significantly affected the catalyst states, resulting in Pt_1/CeO_2 catalysts with distinct Pt_1 states and coordination environments available for different catalytic oxidation reactions (CO oxidation, NH_3 oxidation, *etc.*). More informatively, Pt clusters constructed from Pt_1/CeO_2 with relatively lower $CN_{Pt-O-Ce}$ and weaker Pt−CeO_2 interaction by a facile reduction treatment exhibited much better stability under lean conditions than those evolved from Pt_1 with higher $CN_{Pt-O-Ce}$ and stronger Pt−CeO_2 interactions. It emphasizes again the importance of the initial properties of the catalyst for its evolution under different conditions and implicitly the key to the synthesis procedure. This work provided an easy but effective strategy for developing robust Pt cluster catalysts for CO oxidation under lean conditions.

■ ASSOCIATED CONTENT

Supporting Information

The Supporting Information is available free of charge at https://pubs.acs.org/doi/10.1021/acsami.4c00342.

Details of catalyst characterizations; XRD, N_2-physisorption, ICP-OES, AC-HAADF-STEM, EDS-mapping, XAS, Raman spectra, O_2-TPD, H_2-TPR, and XPS; *in situ* DRIFTS of CO adsorption, CO oxidation, CO-TPD, and NH_3-TPD (PDF)

■ AUTHOR INFORMATION

Corresponding Authors

Wei Tan − *State Key Laboratory of Pollution Control and Resource Reuse, School of Environment, Jiangsu Key Laboratory of Vehicle Emissions Control, Center of Modern Analysis, Nanjing University, Nanjing 210023, China;*

https://doi.org/10.1021/acsami.4c00342
ACS Appl. Mater. Interfaces 2024, 16, 21782−21789

orcid.org/0000-0002-1481-9346; Email: tanwei@nju.edu.cn

Fei Gao − *State Key Laboratory of Pollution Control and Resource Reuse, School of Environment, Jiangsu Key Laboratory of Vehicle Emissions Control, Center of Modern Analysis, Nanjing University, Nanjing 210023, China; School of Environmental Science and Engineering, Nanjing University of Information Science and Technology, Nanjing 210044, China;* orcid.org/0000-0001-8626-5509; Email: fgao@nuist.edu.cn, gaofei@nju.edu.cn

Authors

Peng Yang − *State Key Laboratory of Pollution Control and Resource Reuse, School of Environment, Jiangsu Key Laboratory of Vehicle Emissions Control, Center of Modern Analysis, Nanjing University, Nanjing 210023, China*

Chaoyi Luo − *State Key Laboratory of Pollution Control and Resource Reuse, School of Environment, Jiangsu Key Laboratory of Vehicle Emissions Control, Center of Modern Analysis, Nanjing University, Nanjing 210023, China*

Qinglong Liu − *State Key Laboratory of Pollution Control and Resource Reuse, School of Environment, Jiangsu Key Laboratory of Vehicle Emissions Control, Center of Modern Analysis, Nanjing University, Nanjing 210023, China*

Shaoxiong Zhang − *State Key Laboratory of Pollution Control and Resource Reuse, School of Environment, Jiangsu Key Laboratory of Vehicle Emissions Control, Center of Modern Analysis, Nanjing University, Nanjing 210023, China*

Song Hong − *College of Materials Science and Engineering, Beijing University of Chemical Technology, Beijing 100029, China*

Lin Dong − *State Key Laboratory of Pollution Control and Resource Reuse, School of Environment, Jiangsu Key Laboratory of Vehicle Emissions Control, Center of Modern Analysis, Nanjing University, Nanjing 210023, China;* orcid.org/0000-0002-8393-6669

Complete contact information is available at: https://pubs.acs.org/10.1021/acsami.4c00342

Notes

The authors declare no competing financial interest.

■ ACKNOWLEDGMENTS

This work was supported by the National Natural Science Foundation of China (Nos. 22372076, 22306090, and 21972063) and the Natural Science Foundation of Jiangsu Province (BK20230773).

■ REFERENCES

(1) Pereira-Hernández, X. I.; DeLaRiva, A.; Muravev, V.; Kunwar, D.; Xiong, H.; Sudduth, B.; Engelhard, M.; Kovarik, L.; Hensen, E. J. M.; Wang, Y.; Datye, A. K. Tuning Pt−CeO_2 interactions by high-temperature vapor-phase synthesis for improved reducibility of lattice oxygen. *Nat. Commun.* **2019**, *10* (1), No. 1358.

(2) Tan, W.; Xie, S.; Cai, Y.; Wang, M.; Yu, S.; Low, K. B.; Li, Y.; Ma, L.; Ehrlich, S. N.; Gao, F.; Dong, L.; Liu, F. Transformation of Highly Stable Pt Single Sites on Defect Engineered Ceria into Robust Pt Clusters for Vehicle Emission Control. *Environ. Sci. Technol.* **2021**, *55* (18), 12607−12618.

(3) Gänzler, A. M.; Casapu, M.; Maurer, F.; Störmer, H.; Gerthsen, D.; Ferré, G.; Vernoux, P.; Bornmann, B.; Frahm, R.; Murzin, V.; Nachtegaal, M.; Votsmeier, M.; Grunwaldt, J.-D. Tuning the Pt/CeO_2 Interface by in Situ Variation of the Pt Particle Size. *ACS Catal.* **2018**, *8* (6), 4800−4811.

(4) Ding, C.; Gu, Q.; Yu, L. J.; Zhang, S.; Zhang, Y.; Ma, Z.; Meng, Y.; Zhang, H.; Wang, T.; Wang, J.; Ma, L.; Li, G.; Yang, B.; Zhang, T. Reversible Transformation and Distribution Determination of Diverse Pt Single-Atom Species. *J. Am. Chem. Soc.* **2023**, *145* (4), 2523−2531.

(5) Zhang, Z.; Tian, J.; Lu, Y.; Yang, S.; Jiang, D.; Huang, W.; Li, Y.; Hong, J.; Hoffman, A. S.; Bare, S. R.; Engelhard, M. H.; Datye, A. K.; Wang, Y. Memory-dictated dynamics of single-atom Pt on CeO(2) for CO oxidation. *Nat. Commun.* **2023**, *14* (1), No. 2664.

(6) Xie, S.; Tan, W.; Wang, C.; Arandiyan, H.; Garbrecht, M.; Ma, L.; Ehrlich, S. N.; Xu, P.; Li, Y.; Zhang, Y.; Collier, S.; Deng, J.; Liu, F. Structure-activity relationship of Pt catalyst on engineered ceria-alumina support for CO oxidation. *J. Catal.* **2022**, *405*, 236−248.

(7) Gao, F.; Zhang, Y.; Song, P.; Wang, J.; Song, T.; Wang, C.; Song, L.; Shiraishi, Y.; Du, Y. Precursor-mediated size tuning of monodisperse PtRh nanocubes as efficient electrocatalysts for ethylene glycol oxidation. *J. Mater. Chem. A* **2019**, *7* (13), 7891−7896.

(8) Claudio-Piedras, A.; Ramírez-Zamora, R. M.; Alcántar-Vázquez, B. C.; Gutiérrez-Martínez, A.; Mondragón-Galicia, G.; Morales-Anzures, F.; Pérez-Hernández, R. One dimensional Pt/CeO_2-NR catalysts for hydrogen production by steam reforming of methanol: Effect of Pt precursor. *Catal. Today* **2021**, *360* (1), 55−62.

(9) Tan, W.; Xie, S.; Le, D.; Diao, W.; Wang, M.; Low, K.-B.; Austin, D.; Hong, S.; Gao, F.; Dong, L.; et al. Fine-tuned local coordination environment of Pt single atoms on ceria controls catalytic reactivity. *Nat. Commun.* **2022**, *13* (1), No. 7070.

(10) Zhang, Q.; Mo, S.; Li, J.; Sun, Y.; Zhang, M.; Chen, P.; Fu, M.; Wu, J.; Chen, L.; Ye, D. In situ DRIFT spectroscopy insights into the reaction mechanism of CO and toluene co-oxidation over Pt-based catalysts. *Catal. Sci. Technol.* **2019**, *9* (17), 4538−4551.

(11) Loridant, S. Raman spectroscopy as a powerful tool to characterize ceria-based catalysts. *Catal. Today* **2021**, *373*, 98−111.

(12) Bruix, A.; Lykhach, Y.; Matolinova, I.; Neitzel, A.; Skala, T.; Tsud, N.; Vorokhta, M.; Stetsovych, V.; Sevcikova, K.; Myslivecek, J.; Fiala, R.; Vaclavu, M.; Prince, K. C.; Bruyere, S.; Potin, V.; Illas, F.; Matolin, V.; Libuda, J.; Neyman, K. M. Maximum noble-metal efficiency in catalytic materials: atomically dispersed surface platinum. *Angew. Chem., Int. Ed.* **2014**, *53* (39), 10525−10530.

(13) Dvořák, F.; Camellone, M. F.; Tovt, A.; Tran, N. D.; Negreiros, F. R.; Vorokhta, M.; Skala, T.; Matolinova, I.; Myslivecek, J.; Matolin, V.; Fabris, S. Creating single-atom Pt−Ceria catalysts by surface step decoration. *Nat. Commun.* **2016**, *7*, No. 10801.

(14) Bugrova, T. A.; Kharlamova, T. S.; Svetlichnyi, V. A.; Savel'eva, A. S.; Salaev, M. A.; Mamontov, G. V. Insights into formation of Pt species in Pt/CeO2 catalysts: Effect of treatment conditions and metal-support interaction. *Catal. Today* **2021**, *375*, 36−47.

(15) Wang, C.; Gu, X.-K.; Yan, H.; Lin, Y.; Li, J.; Liu, D.; Li, W.-X.; Lu, J. Water-Mediated Mars−Van Krevelen Mechanism for CO Oxidation on Ceria-Supported Single-Atom Pt_1 Catalyst. *ACS Catal.* **2017**, *7* (1), 887−891.

(16) Nie, L.; Mei, D.; Xiong, H.; Peng, B.; Ren, Z.; Hernandez, X. I. P.; DeLaRiva, A.; Wang, M.; Engelhard, M. H.; Kovarik, L.; Datye, A. K.; Wang, Y. Activation of surface lattice oxygen in single-atom Pt/CeO_2 for low-temperature CO oxidation. *Science* **2017**, *358* (6369), 1419−1423.

(17) Jiao, L.; Regalbuto, J. R. The synthesis of highly dispersed noble and base metals on silica via strong electrostatic adsorption: I. Amorphous silica. *J. Catal.* **2008**, *260* (2), 329−341.